



OPEN ACCESS

EDITED BY

Luigi Aloj,
University of Cambridge, United Kingdom

REVIEWED BY

Roie Manavaki,
University of Cambridge, United Kingdom
Francisco Osvaldo García-Perez,
Instituto Nacional de Cancerología, Mexico

*CORRESPONDENCE

Philippe Thuillier
philippe.thuillier@chu-brest.fr

SPECIALTY SECTION

This article was submitted to PET and SPECT, a section of the journal Frontiers in Nuclear Medicine

RECEIVED 11 May 2022

ACCEPTED 29 August 2022

PUBLISHED 21 September 2022

CITATION

Thuillier P, Bourhis D, Pavoine M, Metges J-P, Le Pennec R, Schick U, Blanc-Béguin F, Hennebicq S, Salaun P-Y, Kerlan V, Karakatsanis NA and Abgral R (2022) Population-based input function (PBIF) applied to dynamic whole-body 68Ga-DOTATOC-PET/CT acquisition. *Front. Nucl. Med.* 2:941848. doi: 10.3389/fnume.2022.941848

COPYRIGHT

© 2022 Thuillier, Bourhis, Pavoine, Metges, Le Pennec, Schick, Blanc-Béguin, Hennebicq, Salaun, Kerlan, Karakatsanis and Abgral. This is an open-access article distributed under the terms of the [Creative Commons Attribution License \(CC BY\)](https://creativecommons.org/licenses/by/4.0/). The use, distribution or reproduction in other forums is permitted, provided the original author(s) and the copyright owner(s) are credited and that the original publication in this journal is cited, in accordance with accepted academic practice. No use, distribution or reproduction is permitted which does not comply with these terms.

Population-based input function (PBIF) applied to dynamic whole-body 68Ga-DOTATOC-PET/CT acquisition

Philippe Thuillier^{1,2*}, David Bourhis^{2,3}, Mathieu Pavoine², Jean-Philippe Metges⁴, Romain Le Pennec^{2,3}, Ulrike Schick⁵, Frédérique Blanc-Béguin^{2,3}, Simon Hennebicq^{2,3}, Pierre-Yves Salaun^{2,3}, Véronique Kerlan^{1,2}, Nicolas A. Karakatsanis⁶ and Ronan Abgral^{2,3}

¹Department of Endocrinology, University Hospital of Brest, Brest, France, ²UMR 1304 Inserm GETBO, University Hospital of Brest, Brest, France, ³Department of Nuclear Medicine, University Hospital of Brest, Brest, France, ⁴Department of Oncology, University Hospital of Brest, Brest, France, ⁵Department of Radiotherapy, University Hospital of Brest, Brest, France, ⁶Department of Radiology, Weil Cornell Medical College of Cornell University, New York, NY, United States

Rational: To validate a population-based input function (PBIF) model that alleviates the need for scanning since injection time in dynamic whole-body (WBdyn) PET.

Methods: Thirty-seven patients with suspected/known well-differentiated neuroendocrine tumors were included (GAPETNET trial NTC03576040). All WBdyn 68Ga-DOTATOC-PET/CT acquisitions were performed on a digital PET system (one heart-centered 6 min-step followed by nine WB-passes). The PBIF model was built from 20 image-derived input functions (IDIFs) obtained from a respective number of patients' WBdyn exams using an automated left-ventricle segmentation tool. All IDIF peaks were aligned to the median time-to-peak, normalized to patient weight and administrated activity, and then fitted to an exponential model function. PBIF was then applied to 17 independent patient studies by scaling it to match the respective IDIF section at 20–55 min post-injection time windows corresponding to WB-passes 3–7. The ratio of area under the curves (AUCs) of IDIFs and PBIF_{3–7} were compared using a Bland–Altman analysis (mean bias ± SD). The Patlak-estimated mean Ki for physiological uptake (Ki-liver and Ki-spleen) and tumor lesions (Ki-tumor) using either IDIF or PBIF were also compared.

Results: The mean AUC ratio (PBIF/IDIF) was 0.98 ± 0.06 . The mean Ki bias between PBIF_{3–7} and IDIF was $-2.6 \pm 6.2\%$ (confidence interval, CI: $-5.8; 0.6$). For Ki-spleen and Ki-tumor, low relative bias with low SD were found [$4.65 \pm 7.59\%$ (CI: 0.26; 9.03) and $3.70 \pm 8.29\%$ (CI: $-1.09; 8.49$) respectively]. For Ki-liver analysis, relative bias and SD were slightly higher [$7.43 \pm 13.13\%$ (CI: $-0.15; 15.01$)].

Conclusion: Our study showed that the PBIF approach allows for reduction in WBdyn DOTATOC-PET/CT acquisition times with a minimum gain of 20 min.

KEYWORDS

neuroendocrine tumor, dynamic whole-body acquisition, 68Ga-DOTATOC-PET/CT, population-based input function, net influx rate

Introduction

Neuroendocrine tumors (NETs) are a group of rare tumors with a common embryological origin (1). NETs are characterized by cellular overexpression of somatostatin receptors (SSTr) allowing the use of radio-labeled somatostatin analogs for diagnostic imaging or peptide-receptor radionuclide therapy. Currently, Gallium-68 DOTA-conjugated somatostatin receptor-targeted peptide (^{68}Ga -DOTA-SSTr) positron emission tomography computed tomography (PET/CT) is the mainstay of well-differentiated NET (WD-NET) diagnosis, staging, and monitoring (2, 3). Dynamic whole-body (WBdyn) acquisition methods in PET imaging have been proposed to assess the spatiotemporal distribution of radiotracers across the human body, allowing calculation of kinetic parameters of clinical relevance, such as the tracer uptake rate K_i using Patlak analysis (4–6). In a recent prospective study, our team showed the feasibility of a WBdyn acquisition in ^{68}Ga -DOTATOC-PET/CT in 61 patients (7). The realization of K_i parametric images required a long dynamic PET acquisition (i.e., 45–60 min depending on the radiotracer) with tracer injection under the PET system to obtain the blood input function and to model time–activity curves in physiological and tumor tissues (8, 9). Currently, several solutions have been developed to make the procedure less constraining such as image-derived input function (IDIF) estimation that is less invasive than venous blood sampling (10, 11). Nevertheless, the main issue in using the Patlak model remains the need to know the time integral of the radiotracer's plasma concentration since injection time throughout the images acquisition (12). One of the current challenges is to reduce this long acquisition time to optimize WBdyn PET studies. Several recent WBdyn ^{18}F -FDG-PET/CT studies have proposed the use of a population-based input function (PBIF) to overcome this key issue (13–19), but to our knowledge, no such data with ^{68}Ga -DOTA-SSTr tracers are available.

The aims of this study were to develop a PBIF model in WBdyn ^{68}Ga -DOTATOC-PET/CT and to validate its clinical use by the most accurate possible estimation of K_i parametric images from fewer WB-passes in a WB-NET independent cohort.

Methods

Patient population

This is an ancillary study of GAPETNET trial (NTC03576040), which is a prospective, observational, and single-center cohort study.

Inclusion criteria were as follows: age ≥ 18 years old; well-differentiated grade 1 or 2 (G1 or G2) neuroendocrine tumor; primary location: gastroenteropancreatic, bronchopulmonary,

or unknown; and WBdyn ^{68}Ga -DOTATOC-PET/CT acquisition performed on digital PET. The protocol was approved by the Institutional Medical Ethics Committee of Brest (29BRC17.0036). Informed consent was obtained from all the patients to participate in the study.

A total of 37 subjects were recruited for this study. The subjects were divided into two groups: a PBIF modeling group ($n = 20$) and an independent validation cohort ($n = 17$).

PET/CT acquisition and image reconstruction

All WBdyn ^{68}Ga -DOTATOC-PET/CT acquisitions were performed on two digital Biograph Vision 600 systems (Siemens©, Erlangen, Germany).

CT acquisition was performed after injection of intravenous iodine contrast agent (1.5 ml/kg), unless contraindicated. The CT consisted of a 64-slice multidetector-row spiral scanner with a transverse field of view of 500 mm. The CT images were reconstructed with an iterative method (SAFIRE, strength 5) for image interpretation. An additional reconstruction of the CT data was performed for attenuation correction using a filtered back projection algorithm and a 780 mm diameter to avoid truncation artifacts.

Dynamic whole-body PET protocol

PET images were then acquired immediately after a manual injection of ^{68}Ga -DOTATOC. The WBdyn PET acquisition was performed according to the methodology previously described by Karakatsanis et al. (5, 6, 9, 20).

A single dynamic cardiac-bed (DCB) position acquisition was followed by a WBdyn craniocaudal continuous bed motion acquisition: 6-min DCB (12 images \times 5 s, 6 images \times 10 s, 8 images \times 30 s) + WBdyn acquisition (9 passes with 2.2 mm/s \approx 54-min duration for the whole WBdyn acquisition).

PET data were first reconstructed with attenuation correction using an iterative reconstruction algorithm (OSEM 3D) with time of flight (ToF) and point spread function (PSF) correction (TrueX). PET images were corrected for random coincidence, scatter, deadtime, normalization, isotope decay, and attenuation using CT data; no smoothing was applied post reconstruction. The size of the transaxial reconstruction was 440×440 (voxel size = $1.65 \text{ mm} \times 1.65 \text{ mm} \times 1.65 \text{ mm}$) with three iterations, five subsets, and 2 mm Gaussian post-filtering. Second, dynamic data were reconstructed using 4D nested direct Patlak reconstruction, matrix 220×220 , four iterations, five subsets, and 3 mm Gaussian post-filtering, thanks to the IDIF or PBIF described below.

Input function

Theoretically, an arterial blood sample is required to obtain an IF, but several studies have shown that it can be estimated only from image data (21–25).

As previously described (26), the total radioactivity concentration in the whole blood is quantified in the reconstructed image and used for the extraction of the IDIF and later for building the PBIF model. A sphere of radius 12 mm was automatically generated as close as possible at the center of the left ventricle and away from the myocardium to mitigate any partial volume effects (26) on both CT series corresponding to DCB and WBdyn acquisitions using an ALPHA [Automated Learning and Parsing of Human Anatomy (27)] algorithm and then applied on PET reconstructed images.

Because we did not performed arterial or venous blood tests during image acquisition, we decided to apply a fixed plasma-to-whole-blood ratio to correct for the IDIF by multiplying by 1.6 the arterial time–activity concentration curve, as previously reported (24, 28).

PBIF creation and IDIF validation cohort

PBIF modeling and fitting (group 1)

The first step was to model a PBIF from the IDIFs of the 20 patients in group 1 as follows: first, all IDIF peaks were aligned to the median time-to-peak (TTP); then, all IDIFs were normalized to the patient's weight and administered activity; finally, the mean IDIF value at each time was used to model the PBIF (Supplementary Figure S1).

The second step was to fit the PBIF using a mathematical model. For this, the PBIF was fitted with a linear interpolation of the concentration before TTP and with an exponential model function using Labfit software® after TTP as follows:

$$SUV(t) = \begin{cases} 0.54(t) - 5.54 & \text{If } t < \text{TTP}, \\ e^{2.27 + \frac{22.33}{t} - 0.47 \ln(t)} & \text{If } t \geq \text{TTP} \end{cases}$$

where t is in seconds.

Validation cohort (group 2)

The third step was to use the modeling PBIF in group 2, including 17 independent patients. The modeled PBIF had to be scaled for each patient and a scaling factor was calculated using the tail part of the IDIF, from the third to seventh passes. For each patient, the PBIF was scaled so that the area under the curve matched the IDIF from the third to seventh WB-passes (PBIF_{3–7}) corresponding approximately to 20–55 min time windows. We used PBIF_{3–7} because Patlak plots

were also calculated from the third to seventh passes of the WBdyn acquisition (7).

An example of the process is illustrated in Supplementary Figure S2.

Patlak reconstruction and Ki extraction

Patlak reconstructions were performed using 4D nested generalized Patlak expectation-maximization reconstruction in the validation cohort, using both IDIF and the scaled PBIFs to obtain parametric images (5, 29–31). Mean Ki-Liver, Ki-spleen, and Ki-tumor values (in ml/min/100 ml) were generated from the different reconstructed parametric images by applying circular 3- and 1-cm diameter region of interests (ROI), respectively, drawn over an uninvaded part of the liver (in the right hepatic lobe) and spleen organs, as previously recommended (32); spherical volume of interests (VOI) drawn over the highest tumor uptake using a fixed threshold method delineating a 3D contour around voxels equal to or greater than 40% of the lesion Ki max, by analogy with the SUV approach. Each ROI and VOI were segmented on the last ninth frame and applied to generate time–activity curves.

An example of parametric images reconstructed using both IDIF and PBIF is represented in the Figure 1.

Statistical analysis

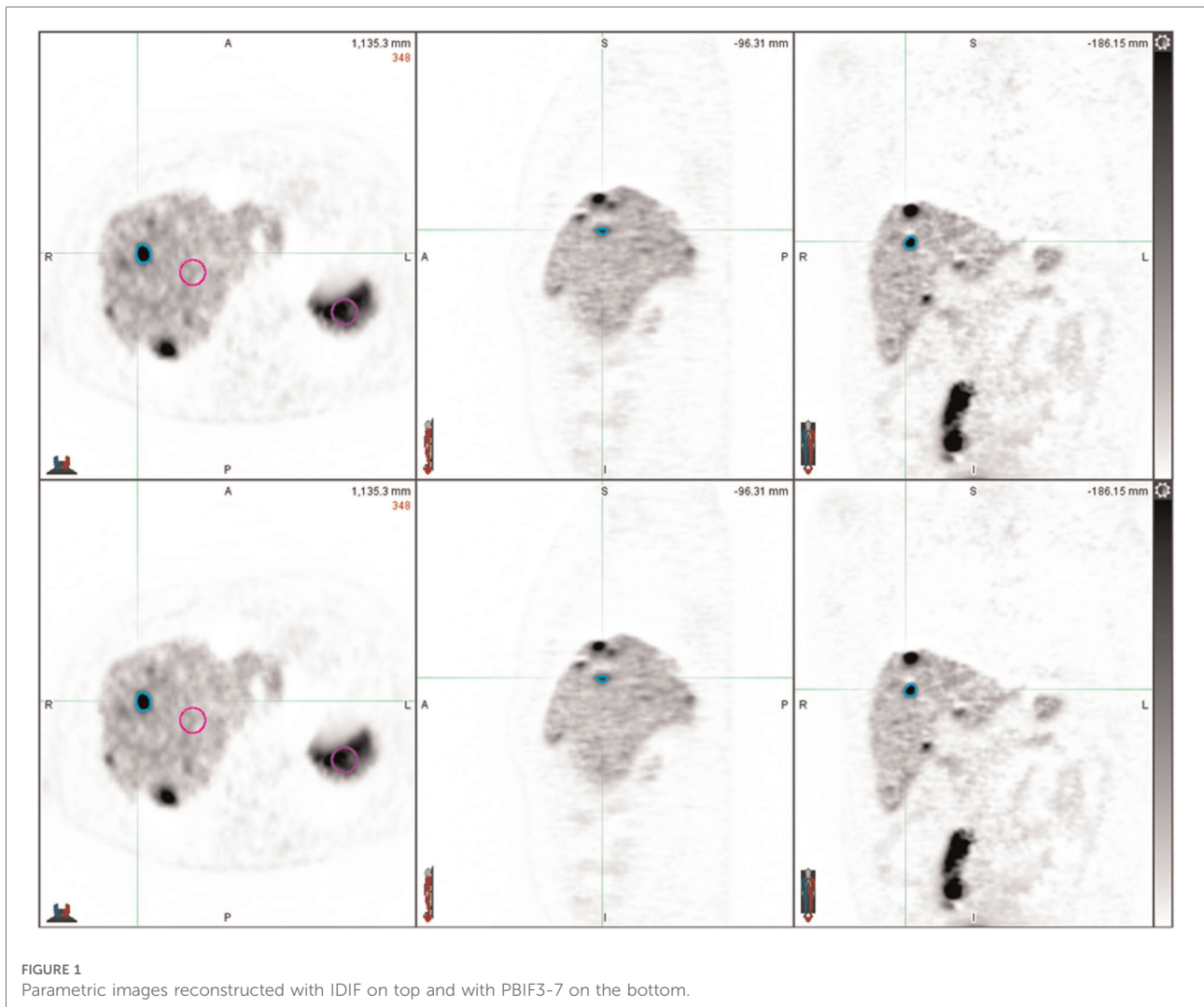
The performance of each scaled PBIF was compared one-by-one to the corresponding IDIF with AUCs. The mean Ki-Liver, Ki-spleen, and Ki-tumor values using both PBIF and IDIF were also compared together. AUC ratio ($AUC_{PBIF/IDIF}$) and Ki ratio ($Ki_{PBIF/IDIF}$) were calculated. Data comparisons were performed using a linear correlation test (R^2 – slope) and a Bland–Altman analysis [mean relative bias; confidence interval (CI) 95%].

The significance level of the p -value was 0.05. All statistical analyses were performed using XLStat 2021 (Addinsoft®, Paris, France) and Excel (Microsoft®, Redmond, Washington, United States) software.

Results

Population

The mean injected tracer doses were 204 ± 45 MBq (range: 136–295) and 2.67 ± 0.29 MBq/Kg (range: 2.02–3.06) in the PBIF modeling group. The mean injected tracer doses were 199 ± 46 MBq (range: 108–287) and 2.81 ± 0.28 MBq/Kg (range: 2.08–3.29) in the validation cohort. There were no significant differences in the demographics parameters (age,



sex ratio, and body mass index) between the PBIF modeling group and the independent validation cohort.

WBdyn PET results

Scaled PBIFs with IDIF comparison

The mean $AUC_{PBIF/IDIF}$ ratio was 0.98 ± 0.06 (range: 0.88–1.11) and $R^2 = 0.96$ (slope = 1.00).

The mean relative bias \pm SD between $PBIF_{3-7}$ and IDIF was $-2.6 \pm 6.2\%$ (CI: $-5.8; 0.6$) (Figure 2).

Ki values analysis

The mean $Ki_{PBIF/IDIF}$ ratio, R^2 correlation coefficient, and mean relative bias \pm SD between PBIF and IDIF are presented in Table 1.

The lowest relative bias \pm SD were found for Ki-tumor [$3.70 \pm 8.29\%$ (CI: $-1.09; 8.49$)] and Ki-spleen [$4.65 \pm 7.59\%$ (CI: $0.26; 9.03$)] metrics comparison (Figures 3A,B). For Ki-liver analysis, the relative bias and SD were slightly higher [$7.43 \pm 13.13\%$ (CI: $-0.15; 15.01$)] (Figure 3C).

Discussion

In our study, we showed the feasibility of using a PBIF to estimate Ki values of WD-NETs from fewer whole-body passes in WBdyn ^{68}Ga -DOTATOC-PET/CT. To our knowledge, this is the first study with such a ^{68}Ga -DOTA-SSTr tracer comparing the PBIF and IDIF approaches for Patlak analysis in WBdyn PET/CT. Implementation of routine WBdyn acquisition for patients with WD-NETs could lead to

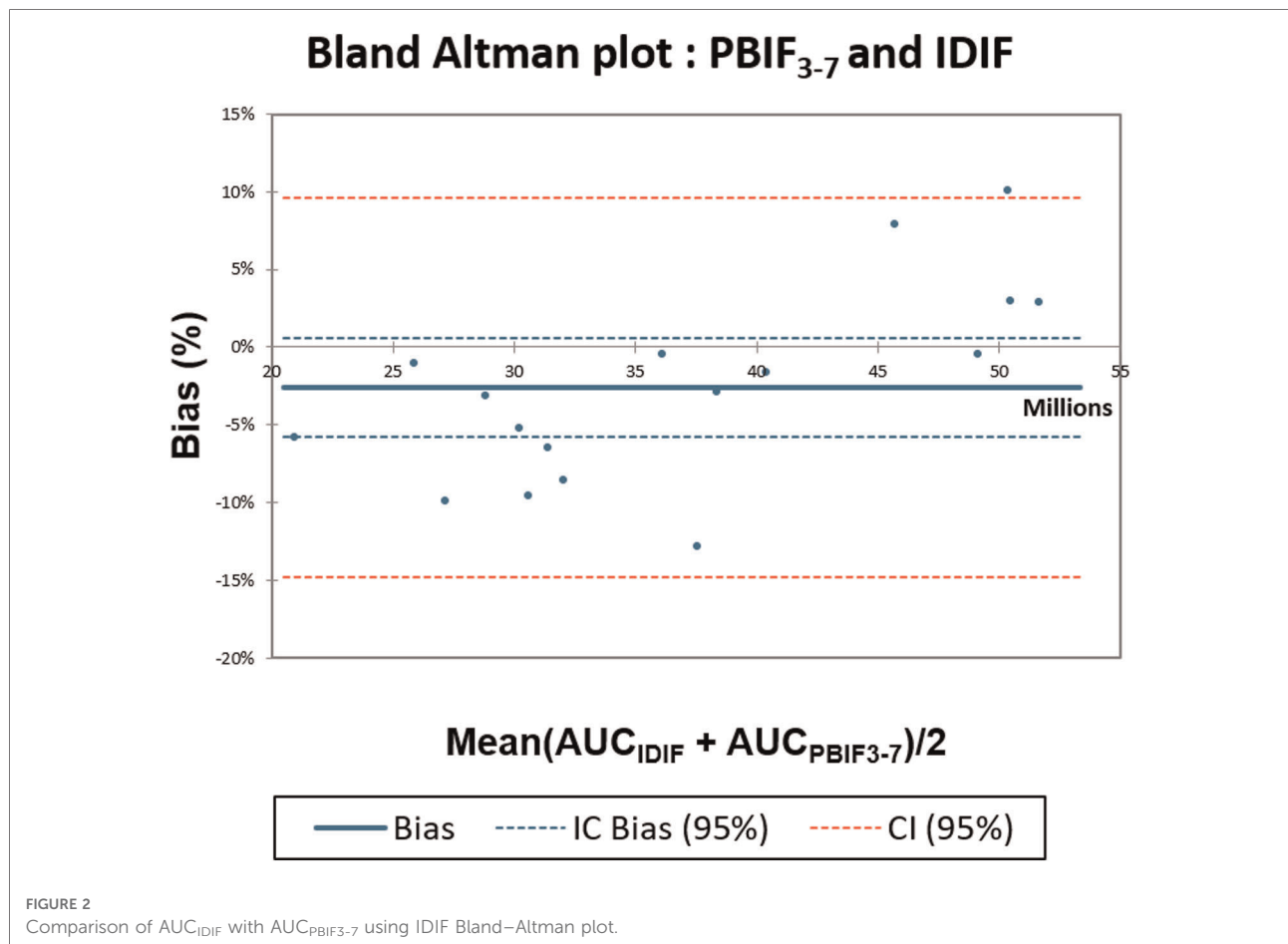


TABLE 1 Mean Ki ratio of Ki-liver, Ki-spleen, and Ki-tumor with results of the correlation test and Bland–Altman analysis between PBIF_{3–7} and IDIF.

	Mean Ki (PBIF/IDIF) [mean ± SD (range)]	Correlation analysis R ² (slope)	Mean relative bias [mean ± SD (CI)]
Ki-liver	1.09 ± 0.14 (0.80–1.31)	0.80 (1.08)	7.43 ± 13.13% (–0.15; 15.01)
Ki-spleen	1.05 ± 0.08 (0.91–1.18)	0.96 (1.05)	4.65 ± 7.59% (0.26; 9.03)
Ki-tumor	1.04 ± 0.09 (0.92–1.26)	1.00 (1.02)	3.70 ± 8.29% (–1.09; 8.49)

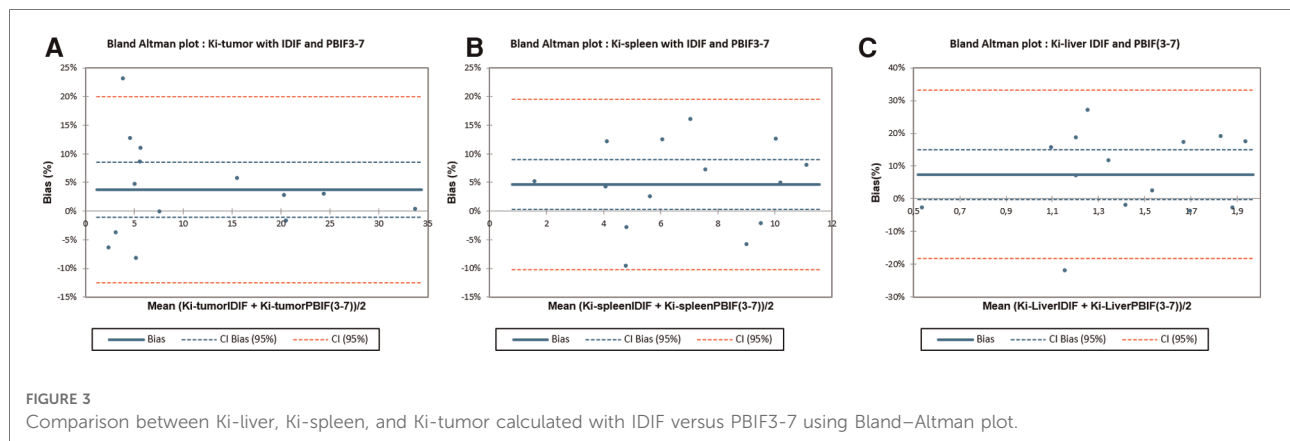
PBIF, population-based input function; IDIF, image-derived input function; CI, confidence interval.

a better characterization of the physiological and tumoral tracer uptake in the future, providing *in vivo* additional quantitative value in the characterization of SSTR expression in WD-NETs as previously reported (7).

Regarding the comparison between IDIF and scaled PBIF_{3–7}, we found a low bias [AUC ratio = 0.98 ± 0.06, R² = 0.96 (slope

= 1.00), mean bias –2.6 ± 6.2%]. In comparison with literature data, Naganawa et al. compared IDIF and PBIF in oncological WBdyn 18F-FDG-PET/CT studies with the gold standard as an arterial input function (AIF). The authors highlighted that using the PBIF on 15–45 and 30–60 min time windows allowed us to obtain respective mean bias of –1 ± 6% (R² = 0.93) and 3 ± 6% (R² = 0.94) compared to AIF (13). These time windows are finally quite like the one used in our study (20–55 min). Moreover, they found similar results in using the IDIF with a bias of –1 ± 5% (R² = 0.91). However, the choice of later time windows (45–75 and 60–90 min) led to an overestimation of the AIF in their series [mean bias of 9 ± 7%, (R² = 0.93) and 19 ± 10% (R² = 0.88), respectively]. Therefore, we can assume that in terms of AUC ratio, using a 3–7 time window does not lead to a significant overall impact compared to IDIF.

Our results showed excellent results for Ki-tumor estimation with PBIF providing low bias with low standard deviation. Moreover, the confidence interval of this relative bias included the value 0 in our comparison [bias = 3.70 ± 8.29% (CI: –1.09; 8.49)] that is of major importance in a context of optimizing the characterization of NETs in



68Ga-DOTATOC-PET/CT. In a recent study including 14 patients with lung cancer, Indovina et al. found similar results on Ki-metrics estimation using a PBIF model scaled on a 40–60 min time window in WBdyn 18F-FDG-PET/CT (correlation of mean Ki_{IDIF} and Ki_{PBIF} values of $R^2 = 0.997$) (14).

We also studied physiological Ki-metrics because spleen and liver uptakes were historically used in scintigraphy to estimate SSTR density expression in NETs (33). Using PBIF₃₋₇, we found relatively same results for Ki-spleen than for Ki-tumor estimation with a low relative bias [Ki ratio = 1.05 ± 0.08 , $R^2 = 0.96$ (slope = 1.05), bias = $4.66 \pm 7.59\%$ (CI: 0.26; 9.03)]. However, for Ki-liver analysis, we found a positive bias with higher SD of $7.43 \pm 13.13\%$. In our cohort, mean Ki-liver values were lower to the mean Ki-spleen and Ki-tumor values in our 17 scans (1.35 ± 0.36 , 6.65 ± 2.77 , and 11.09 ± 9.87 ml/min/100 ml, respectively). So, we assume that higher variance of bias in our Ki-liver analysis is mainly related to their low values, whose small changes had a greater impact in modeling the input function. Finally, it might also be explained by physiological motion of such organ (i.e., breathing) during data acquisition.

Our study has several limitations. First, we did not perform arterial blood sample for PBIF scaling. Hence, our analysis allows only a comparison to the IDIF-based approach. Therefore, we cannot conclude whether the use of PBIF results in more accurate estimation of Ki values compared to the AIF gold standard. However, we applied a fixed plasma-to-whole-blood ratio of 1.6 to correct for the IDIF as previously reported, which leads to estimate accurately the Ki values without performing iterative arterial or venous blood tests during image acquisition (24). Furthermore, we only used the WB-passes time window proposed by our reconstruction software. The comparison of results using different time windows will be the topic of a future publication to find out what is

the best compromise between the acquisition time duration and the most optimized PBIF in terms of bias and variance. Finally, due to the relatively small number of patients, we did not perform subgroup analysis such as with patient age- or gender-specific IFs that could improve the accuracy of the PBIF modeling.

Conclusion

Our study showed that the PBIF approach allows for a reduction in WBdyn DOTATOC-PET/CT acquisition time, allowing a minimum time gain of 20 min using WB-passes 3–7 and thereby facilitating its use in routine clinical practice. Further evaluation with a larger dataset is needed to confirm these promising results.

Data availability statement

The raw data supporting the conclusions of this article will be made available by the authors, without undue reservation.

Ethics statement

The study (NCT03576040) was approved by our University Hospital's Institutional Review Board of Brest (29BRC17.0036). The patients/participants provided their written informed consent to participate in this study.

Author contributions

VK, P-YS, and RA are the guarantors of the paper. PT, DB, NAK, and RA designed the study. PT realized statistics. J-PM

and PT ensured the follow-up of patients. FB-B and SH ensured the preparation of the radiotracer. PT, NAK, and RA drafted the manuscript. PT, DB, RA, and MP did the interpretation of data. VK, P-YS, RA, NAK, RLP, and US revised the manuscript for intellectual content. All authors contributed to the article and approved the submitted version.

Conflict of interest

The authors declare that the research was conducted in the absence of any commercial or financial relationships that could be construed as a potential conflict of interest.

Publisher's note

All claims expressed in this article are solely those of the authors and do not necessarily represent those of their affiliated organizations, or those of the publisher, the editors

and the reviewers. Any product that may be evaluated in this article, or claim that may be made by its manufacturer, is not guaranteed or endorsed by the publisher.

Supplementary material

The Supplementary Material for this article can be found online at: <https://www.frontiersin.org/articles/10.3389/fnume.2022.941848/full#supplementary-material>.

Supplementary Figure 1

Mean \pm SD of the 20 IDIFs of the group 1 and corresponding modeled PBIF.

Supplementary Figure 2

Example of nonscaled PBIF and IDIF for the full acquisition (top) and the scaled PBIF using 3–7 pass points from the IDIF (bottom).

Supplementary Table 1

General characteristics of the PBIF creation (group 1) and IDIF validation population (group 2).

References

- Modlin IM, Oberg K, Chung DC, Jensen RT, de Herder WW, Thakker RV, et al. Gastroenteropancreatic neuroendocrine tumours. *Lancet Oncol.* (2008) 9:61–72. doi: 10.1016/S1470-2045(07)70410-2
- Barrio M, Czernin J, Fanti S, Ambrosini V, Binse I, Du L, et al. The impact of somatostatin receptor-directed PET/CT on the management of patients with neuroendocrine tumor: a systematic review and meta-analysis. *J Nucl Med.* (2017) 58:756–61. doi: 10.2967/jnumed.116.185587
- Graham MM, Gu X, Ginader T, Breheny P, Sunderland JJ. ⁶⁸Ga-DOTATOC imaging of neuroendocrine tumors: a systematic review and metaanalysis. *J Nucl Med.* (2017) 58:1452–8. doi: 10.2967/jnumed.117.191197
- Patlak CS, Blasberg RG, Fenstermacher JD. Graphical evaluation of blood-to-brain transfer constants from multiple-time uptake data. *J Cereb Blood Flow Metab.* (1983) 3:1–7. doi: 10.1038/jcbfm.1983.1
- Karakatsanis NA, Zhou Y, Lodge MA, Casey ME, Wahl RL, Zaidi H, et al. Generalized whole-body Patlak parametric imaging for enhanced quantification in clinical PET. *Phys Med Biol.* (2015) 60:8643–73. doi: 10.1088/0031-9155/60/22/8643
- Karakatsanis NA, Lodge MA, Zhou Y, Mhlanga J, Chaudhry MA, Tahari AK, et al. *Dynamic multi-bed FDG PET imaging: feasibility and optimization.* in 2011 IEEE Nuclear Science Symposium and Medical Imaging Conference (NSS/MIC). Valencia, Spain: IEEE Nuclear Science Symposium Conference Record (2011). p. 3863–70.
- Thuillier P. Prospective study of dynamic whole-body ⁶⁸Ga-DOTATOC-PET/CT acquisition in patients with well-differentiated neuroendocrine tumors. *Sci Rep.* (2021) 11:4727. doi: 10.1038/s41598-021-83965-9
- Karakatsanis NA, Lodge MA, Casey ME, Zaidi H, Rahmim A. *Impact of acquisition time-window on clinical whole-body PET parametric imaging.* 2014 IEEE Nuclear Science Symposium and Medical Imaging Conference (NSS/MIC). Seattle, WA, USA: IEEE (2014). p. 1–8.
- Karakatsanis NA, Lodge MA, Zhou Y, Wahl RL, Rahmim A. Dynamic whole-body PET parametric imaging: II. Task-oriented statistical estimation. *Phys Med Biol.* (2013) 58:7419–45. doi: 10.1088/0031-9155/58/20/7419
- Zanotti-Fregonara P, Chen K, Liow J-S, Fujita M, Innis RB. Image-derived input function for brain PET studies: many challenges and few opportunities. *J Cereb Blood Flow Metab.* (2011) 31:1986–98. doi: 10.1038/jcbfm.2011.107
- Zanotti-Fregonara P, Fadaili EM, Maroy R, Comtat C, Souloumiac A, Jan S, et al. Comparison of eight methods for the estimation of the image-derived input function in dynamic [(18)F]-FDG PET human brain studies. *J Cereb Blood Flow Metab.* (2009) 29:1825–35. doi: 10.1038/jcbfm.2009.93
- Patlak CS, Blasberg RG. Graphical evaluation of blood-to-brain transfer constants from multiple-time uptake data. *J Cereb Blood Flow Metab.* (1985) 5:584–90. doi: 10.1038/jcbfm.1985.87
- Naganawa M, Gallezot J-D, Shah V, Mulnix T, Young C, Dias M, et al. Assessment of population-based input functions for Patlak imaging of whole body dynamic ¹⁸F-FDG PET. *EJNMMI Phys.* (2020) 7:67. doi: 10.1186/s40658-020-00330-x
- Indovina L, Scolozzi V, Capotosti A, Sestini S, Taralli S, Cusumano D, et al. Short 2-[¹⁸F]fluoro-2-deoxy-D-glucose PET dynamic acquisition protocol to evaluate the influx rate constant by regional Patlak graphical analysis in patients with non-small-cell lung cancer. *Front Med.* (2021) 8:725387. doi: 10.3389/fmed.2021.725387
- Karakatsanis N, Zhou Y, Lodge M, Casey M, Wahl R, Subramaniam R, et al. Clinical whole-body PET Patlak imaging 60–90 min post-injection employing a population-based input function. *J Nucl Med.* (2015) 56:1786. doi: 10.2967/jnumed.115.156364
- Karakatsanis N, Lodge M, Zhou Y, Casey M, Wahl R, Subramaniam R, et al. Novel multi-parametric SUV/patlak FDG-PET whole-body imaging framework for routine application to clinical oncology. *J Nucl Med.* (2015) 56:625. https://jnm.snmjournals.org/content/56/supplement_3/625
- van Sluis J, Yaqub M, Brouwers AH, Dierckx RAJO, Noordzij W, Boellaard R. Use of population input functions for reduced scan duration whole-body Patlak 18F-FDG PET imaging. *EJNMMI Phys.* (2021) 8:11. doi: 10.1186/s40658-021-00357-8
- Yao S, Feng T, Zhao Y, Wu R, Wang R, Wu S, et al. Simplified protocol for whole-body Patlak parametric imaging with 18 F-FDG PET/CT: feasibility and error analysis. *Med Phys.* (2021) 48:2160–9. doi: 10.1002/mp.14187
- Wu Y, Feng T, Zhao Y, Xu T, Fu F, Huang Z, et al. Whole-body parametric imaging of 18F-FDG PET using uEXPLORER with reduced scanning time. *J Nucl Med.* (2022) 63:622–8. doi: 10.2967/jnumed.120.261651
- Karakatsanis NA, Lodge MA, Tahari AK, Zhou Y, Wahl RL, Rahmim A. Dynamic whole-body PET parametric imaging: I. Concept, acquisition protocol optimization and clinical application. *Phys Med Biol.* (2013) 58:7391–418. doi: 10.1088/0031-9155/58/20/7391
- Van Binnebeek S, Koole M, Terwinghe C, Baete K, Vanbilloen B, Haustermans K, et al. Dynamic ⁶⁸Ga-DOTATOC PET/CT and static image in

- NET patients. Correlation of parameters during PRRT. *Nuklearmedizin*. (2016) 55:104–14. doi: 10.3413/Nukmed-0742-15-05
22. Henze M, Schuhmacher J, Hipp P, Kowalski J, Becker DW, Doll J, et al. PET imaging of somatostatin receptors using [68Ga]DOTA-D-Phe1-Tyr3-octreotide: first results in patients with meningiomas. *J Nucl Med*. (2001) 42:1053–6. <https://jnm.snmjournals.org/content/42/7/1053>
23. Koukouraki S, Strauss LG, Georgoulas V, Eisenhut M, Haberkorn U, Dimitrakopoulou-Strauss A. Comparison of the pharmacokinetics of 68Ga-DOTATOC and [18F]FDG in patients with metastatic neuroendocrine tumours scheduled for 90Y-DOTATOC therapy. *Eur J Nucl Med Mol Imaging*. (2006) 33:1115–22. doi: 10.1007/s00259-006-0110-x
24. Jahn U, Ilan E, Velikyan I, Fröss-Baron K, Lubberink M, Sundin A. Receptor depletion and recovery in small-intestinal neuroendocrine tumors and normal tissues after administration of a single intravenous dose of octreotide measured by 68Ga-DOTATOC PET/CT. *EJNMMI Res*. (2021) 11:118. doi: 10.1186/s13550-021-00860-0
25. Ivanidze J, Roytman M, Skafida M, Kim S, Glynn S, Osborne JR, et al. Dynamic 68Ga-DOTATATE PET/MRI in the diagnosis and management of intracranial meningiomas. *Radiol Imaging Cancer*. (2022) 4:e210067. doi: 10.1148/rycan.210067
26. Chen K, Bandy D, Reiman E, Huang SC, Lawson M, Feng D, et al. Noninvasive quantification of the cerebral metabolic rate for glucose using positron emission tomography, 18F-fluoro-2-deoxyglucose, the Patlak method, and an image-derived input function. *J Cereb Blood Flow Metab*. (1998) 18:716–23. doi: 10.1097/00004647-199807000-00002
27. Shah V. “Automatic landmarking and parsing of human anatomy (ALPHA) for innovative and smart MI applications.” Siemens WhitePaper.
28. Ilan E, Velikyan I, Sandström M, Sundin A, Lubberink M. Tumor-to-blood ratio for assessment of somatostatin receptor density in neuroendocrine tumors using 68Ga-DOTATOC and 68Ga-DOTATATE. *J Nucl Med*. (2020) 61:217–21. doi: 10.2967/jnumed.119.228072
29. Karakatsanis NA, Casey ME, Lodge MA, Rahmim A, Zaidi H. Whole-body direct 4D parametric PET imaging employing nested generalized Patlak expectation-maximization reconstruction. *Phys Med Biol*. (2016) 61:5456–85. doi: 10.1088/0031-9155/61/15/5456
30. Hu J, Panin V, Smith AM, Spottiswoode B, Shah V, von Gall CC, et al. Design and implementation of automated clinical whole body parametric PET with continuous bed motion. *IEEE Trans Radiat Plasma Med Sci*. (2020) 4:696–707. doi: 10.1109/TRPMS.2020.2994316
31. Karakatsanis N, Lodge M, Wahl R, Rahmim A. Direct 4D whole-body PET/CT parametric image reconstruction: concept and comparison vs. indirect parametric imaging. *J Nucl Med*. (2013) 54:2133. https://jnm.snmjournals.org/content/54/supplement_2/2133
32. Thuillier P, Maajem M, Schick U, Blanc-Beguín F, Hennebicq S, Metges J-P, et al. Clinical assessment of 177Lu-DOTATATE quantification by comparison of SUV-based parameters measured on both post-PRRT SPECT/CT and 68Ga-DOTATOC PET/CT in patients with neuroendocrine tumors: a feasibility study. *Clin Nucl Med*. (2020) 46:111–8. doi: 10.1097/RLU.00000000000003412
33. Krenning EP, Kwekkeboom DJ, Bakker WH, Breeman WA, Kooij PP, Oei HY, et al. Somatostatin receptor scintigraphy with [111In-DTPA-D-Phe1]- and [123I-Tyr3]-octreotide: the Rotterdam experience with more than 1000 patients. *Eur J Nucl Med*. (1993) 20:716–31. doi: 10.1007/BF00181765